Compensation of Anisotropy in Spin Hall Devices for Neuromorphic Applications

Pankaj Sethi, Dédalo Sanz-Hernández, Florian Godel, Sachin Krishnia, Fernando Ajejas, Alice Mizrahi, Vincent Cros, Danijela Marković, and Julie Grollier

Compensation of anisotropy in spin-Hall devices for fixed frequency applications

Pankaj Sethi*, Dédalo Sanz-Hernández, Florian Godel, Sachin Krishnia, Fernando Ajejas[a],
Alice Mizrahi, Vincent Cros, Danijela Marković and Julie Grollier

Unité Mixte de Physique CNRS/Thales, Université Paris-Saclay, 91767 Palaiseau, France

Spintronic nano-oscillators and diodes with reduced non-linearity benefit from low phase noise and improved device properties. Moreover, they could offer key advantages for realizing neuromorphic applications such as spike-based neurons and frequency multiplexing in neural networks. Here, we experimentally demonstrate the reduction in non-linearity of a spin-Hall nano-oscillator (SHNO) by compensation of its effective magnetic anisotropy. The study involves optimization of Co/Ni multilayer growth to achieve the compensation, followed by spin diode measurements on patterned microstrips to quantify their anisotropy. The relation between the second ($H_{k2} = 0.47$ mT) and the first order ($H_{k1}^{eff} = -0.8$ mT) anisotropy fields reveals the existence of an easy cone, thereby validating the presence of compensation. Furthermore, we demonstrate a compensated spin diode which has a fixed frequency when the input power is varied. We then study the current-induced auto-oscillation properties of SHNOs on compensated films by patterning nano-constrictions of widths 200 and 100 nm. The invariance of the resonance frequency and linewidth of the compensated SHNO with applied dc current indicates the absence of non-linearity. This independence is maintained irrespective of the applied external fields and its orientations. The compensated SHNO obtained has a linewidth of 1.1 MHz and a peak output power of up to 1 pW/MHz.

[a] Present address: Department of Physics and Center for Advanced Nanoscience, University of California, San Diego, La Jolla, CA, 92093, USA

*Corresponding author: pankaj.sethi@cnrs-thales.fr, pankaj8684@gmail.com

I. INTRODUCTION

Spintronic nano-oscillators are nano-scale microwave generators which undergo auto-oscillations when the spin transfer or the spin orbit torque, due to the applied dc current, counteracts the damping due to the magnetization precession [1–4]. Non-linearity is prevalent in the magnetization dynamics of such nano-oscillators. In a non-linear auto-oscillator, the frequency, f, has a component which depends on the precession amplitude or the effective magnetization given by,

$$f = f_{FMR} + Np,$$ (1)

where f_{FMR} is the frequency at ferromagnetic resonance, N is the non-linear frequency shift coefficient and p is the term related to the amplitude of precession [5,6]. It is worth noting that even in the complete absence of non-linearity ($N = 0$), the frequency of the oscillators could still be offset from f_{FMR} on account of internal fields. These internal fields could arise, for instance, due to the device geometry, as was demonstrated in [7] for spin Hall oscillators based on nano-constriction geometries. The non-linear frequency shit, N, emerges from an effective anisotropy in the system, which results in non-circular trajectory of the precessing magnetization. The magnetization dynamics in the ferromagnetic layer are inherently non-linear due to the non-linear relationship between the applied magnetic field, the magnetization and the resulting precession frequency. This non-linearity affects the frequency response of the spintronic nano-oscillator, causing it to depend on the precession amplitude [6]. It leads to a large frequency tunability with current which provides multifunctionality to these nano-oscillators such as the possibility to be modulated or synchronized [8–10]. This has been exploited in realizing numerous applications relevant to data communication [11–15] and neuromorphic computing [16–19]. However, there are certain systems where it is possible to reduce the effective anisotropy and, as a result, the non-linearity. In such compensated systems, the anisotropy field is counterbalanced by the demagnetization field, resulting in circular trajectories of the precessing magnetization [20]. The absence of nonlinearity, which results in a constant frequency with respect to the injected input power or current, also offers key benefits for realizing neuromorphic applications. For instance, multiply-and-accumulate (MAC) operations using spintronic resonators employ frequency multiplexing to uniquely address input radio frequency (RF) signals from neurons to the corresponding resonators [21,22]. This requires the neurons and the corresponding spin diode-based synapses to resonate at a relatively fixed frequency independent of the injected RF power. This paper will show that fixed

2

frequency operation can be accomplished by compensating anisotropy in spintronic nano-oscillators and spin diodes, respectively. Secondly, an absence of non-linearity can reduce the phase noise of the nano-oscillator by removing the effect of amplitude noise on it. The linewidth, Δf, of an auto-oscillator, which is a measure of its phase noise [23] is given by,

$$\Delta f = \Delta f_{thermal} \left(1 + N^2/\Gamma_{eff}^2\right), \tag{2}$$

where $\Delta f_{thermal}$ is the contribution from the thermal generation linewidth and Γ_{eff} is the effective damping [5]. The second term, which is the contribution from the amplitude noise, can be neglected if N is very small. Another application is the realization of spike-based neurons which was recently demonstrated via macro-spin approach and micromagnetic simulations [24]. It was shown that anisotropy compensation in a spin Hall geometry results in circular trajectories of the precessing magnetization and the resulting output is a chain of spikes emulating the biological neurons. Thus, it is important to study systems with compensated anisotropy.

Recently, Jiang *et al.* have demonstrated a linewidth reduction of spin-valve based spin-torque nano-oscillators (STNOs) by controlling the perpendicular magnetic anisotropy (PMA) of their films using He-ion irradiation [25]. An alternate planar geometry based on heavy metal and ferromagnetic layers, which utilizes spin current injected from the heavy metal by spin Hall effect to sustain precession in the ferromagnet, benefits from ease of fabrication [26–28]. Moreover, spin Hall nano-oscillators (SHNOs), in the form of a nano-constriction geometry of these layers, exhibit auto-oscillations by way of mode confinement in a potential well formed by non-uniform magnetic field [29–31]. Divinskiy *et al.* demonstrated the suppression of nonlinear damping by compensation of in-plane dipolar anisotropy with PMA in Co/Ni based disks patterned on Pt heavy metal [32]. However, the detection of auto-oscillations was performed by optical methods which are less suitable for on chip applications.

Usually, in systems with an interfacial anisotropy, the first order anisotropy (K_1) dominates over the second order anisotropy (K_2). However, close to the spin re-orientation, when the demagnetization field counter-balances the first order anisotropy field, K_2 also starts to play a crucial role. In this case, magnetization prefers to align itself along a continuous cone of directions instead of a single axis. The easy cone has been exploited to reduce the switching current of magnetic tunnel junction (MTJ) based memory devices [33–35], but to the best of our knowledge, a demonstration of easy cone for the reduction of non-linearity in SHNOs is still lacking.

Here, we experimentally demonstrate, by all-electrical measurements, a reduction of non-linearity and linewidth of an SHNO, based on Co/Ni multilayers with compensated anisotropy and a Pt heavy metal layer. Compensation is achieved by tuning the thicknesses of the Co/Ni multilayers. The effective anisotropy is estimated using spin diode measurements performed on microstrip waveguides. The relation between the second and the first order anisotropy terms indicate the presence of an easy cone state which validates the existence of compensation. The compensated spin diode thus obtained, does not show variation of its frequency with the injected RF power and can potentially function as a synapse. Nano-constriction based SHNOs with different widths are then patterned on the compensated stacks and the output microwave spectra are analysed. The frequency is found to remain nearly constant as a function of dc current for a wide range of magnetic field strengths and orientations. Moreover, an extremely low linewidth close to 1 MHz (quality factor = 7500) is obtained, which does not increase significantly at large applied dc currents. In contrast, as a control an SHNO was fabricated with an in-plane anisotropy $Ni_{81}Fe_{19}$/Pt stack, which exhibits significant shift of frequency and linewidth with the applied dc current.

II. COMPENSATION OF ANISOTROPY IN SPIN HALL DEVICES

A. Sample preparation

The stacks consisting of Ta (5) /Pt (6) /[Co (x) /Ni (y)]$_5$ /Co (x) /Al (2) (thicknesses are in nm) are deposited on high resistivity Silicon (001) substrates (resistivity > 10000 Ω-cm) by dc-magnetron sputtering at room temperature. Ta is used as a seed layer to promote adhesion between silicon and the subsequent layer and Pt serves as the heavy metal layer. Co/Ni multilayers are chosen for their large PMA and spin polarization which can be tuned by varying layer thicknesses [36], as demonstrated previously for domain-wall based devices [37,38]. A Co/Ni multilayer repetition of five was chosen to obtain a sizeable absolute magnetization [39]. Thicknesses of Co (x) and Ni (y) are varied to tune the anisotropy and the corresponding M-H loops are measured for in-plane (IP) and out-of-plane (OOP) field orientations using alternating gradient force magnetometry (AGFM). Starting with in-plane anisotropy (IPA) for Co (0.5 nm)

and Ni (0.8 nm) [Fig. 1(a)], the thickness of Co is reduced to 0.4 nm and PMA is obtained [Fig. 1(c)] due to interfacial anisotropy overcoming the demagnetization field. Henceforth, in this article, Co (0.5 nm) /Ni (0.8 nm) and Co (0.4 nm) /Ni (0.8 nm) multilayers are referred to as IPA and PMA stacks, respectively. Further, when the thickness of Ni is increased to 0.9 nm, the PMA reduces but the anisotropy is neither fully in-plane nor out-of-plane [Fig. 1(b)]. As will be described in what follows, the intermediate anisotropy obtained with Co (0.4 nm) and Ni (0.9 nm) has been compensated and this film is referred to as the compensated stack. The anisotropy fields were extracted using spin diode measurements [27,40]. To carry out the measurements, the multilayers were patterned into microstrip waveguides of width 10 µm and length 25 µm using optical lithography and Ar ion beam etching techniques. Ti (15 nm)/Au (150 nm) metal stacks are deposited as electrodes and patterned into coplanar waveguides overlaying the microstrips using optical lithography and lift-off techniques. The resulting samples are henceforth referred as IPA, PMA and compensated devices, respectively.
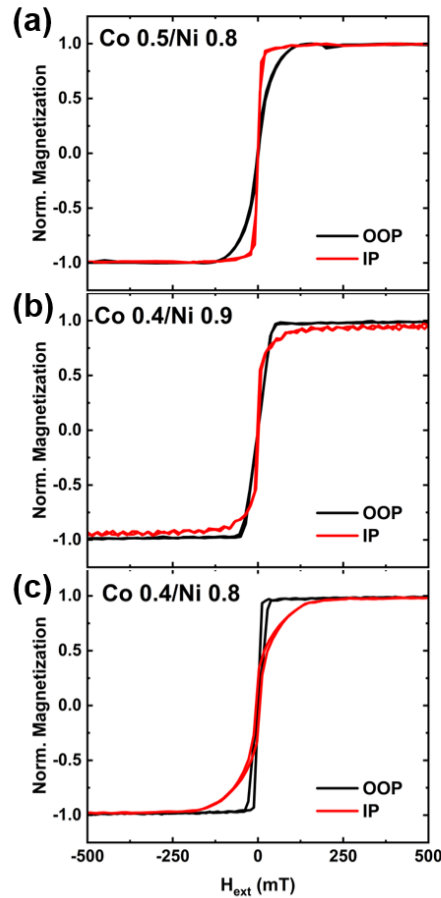

FIG. 1. Alternating gradient magnetometry measurements for Ta (5) /Pt (6)/ [Co (x) / Ni (y)]5/ Co (x)/ Al (2) (thicknesses are in nm) films with (a) in-plane anisotropy (x = 0.5, y = 0.8), (b) compensated anisotropy (x = 0.4, y = 0.9) and (c) perpendicular anisotropy (x = 0.4, y = 0.8).

B. Spin-diode measurements and estimation of effective anisotropy

Figure 2 shows the spin-diode measurement set-up. A microwave current with a power of 8 mW (9 dBm) is injected into the microstrip device to generate microwave frequency spin-orbit torque (SOT) on the ferromagnetic layers due to the heavy metal Pt [27]. The mixing between the oscillating magneto-resistance and the microwave current produces a dc rectified voltage, V_{dc}, at the ferromagnetic resonance, which is detected by using a lock-in amplifier. The external field is swept close to the OOP direction for the PMA device (θ = 5 deg) and is swept IP (φ = 45 deg) for the compensated and IPA devices, where θ and φ are the polar and azimuthal angles, respectively. By keeping the field orientation close to the anisotropy of the devices we can eliminate the artefacts due to geometry induced local anisotropy variation and simplify the analysis [41]. All measurements are performed at room temperature. Resonance plots obtained for the PMA, the compensated and the IPA devices are shown in Figures 3 (a), (b) and (c), respectively. The amplitudes observed in the resonance plots are not corrected for the non-flat frequency response of the wire bonds and the cabling in the set-up. However, in our analysis we are only interested in the estimation of the resonance fields which are independent of amplitude losses. The plots can be well fit by the sum of symmetric and antisymmetric Lorentzian curves [27]. The resonance field, H_r is extracted for each of the injected microwave frequency (f_{res}) and the Kittel functions (f_{res} vs H_r) are plotted for each of the three configurations. The linear relation obtained in Figure 3 (d) for the PMA device is well explained by the Kittel formula, $f_{res} = \gamma/2\pi(H_r - \mu_0 M_{eff})$ [42], where
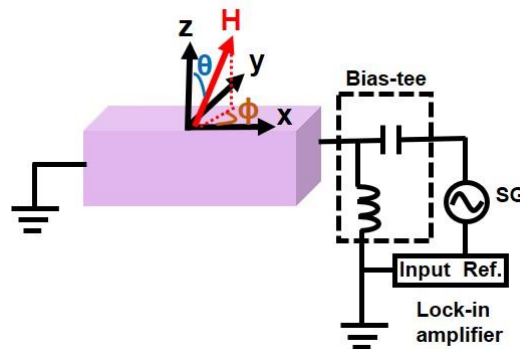

FIG. 2. Schematic illustration of spin-diode measurement set-up

$\mu_0 M_{eff} = \mu_0 M_s - H_k$, is the effective anisotropy field; symbols γ, μ_0, M_s, H_k denote the gyromagnetic ratio, vacuum permeability, saturation magnetization and perpendicular anisotropy field, respectively. The fit of the equation yields an $M_{eff} = -35$ mT. The negative sign of M_{eff} confirms the existence of PMA. Figures 3 (e) and (f) depict the f_{res} vs H_r plots for the compensated and the IPA devices, respectively which are well fit with the equation, $f_{res} = \gamma/2\pi[H_r(H_r + \mu_0 M_{eff})]^{1/2}$ [27]. The extracted values of M_{eff} are 0.5 mT and +86.6 mT for the compensated and the IPA devices, respectively. As a comparison, the Kittel function corresponding to $M_{eff} = 0$ is also plotted together with the as obtained fits for each of the three
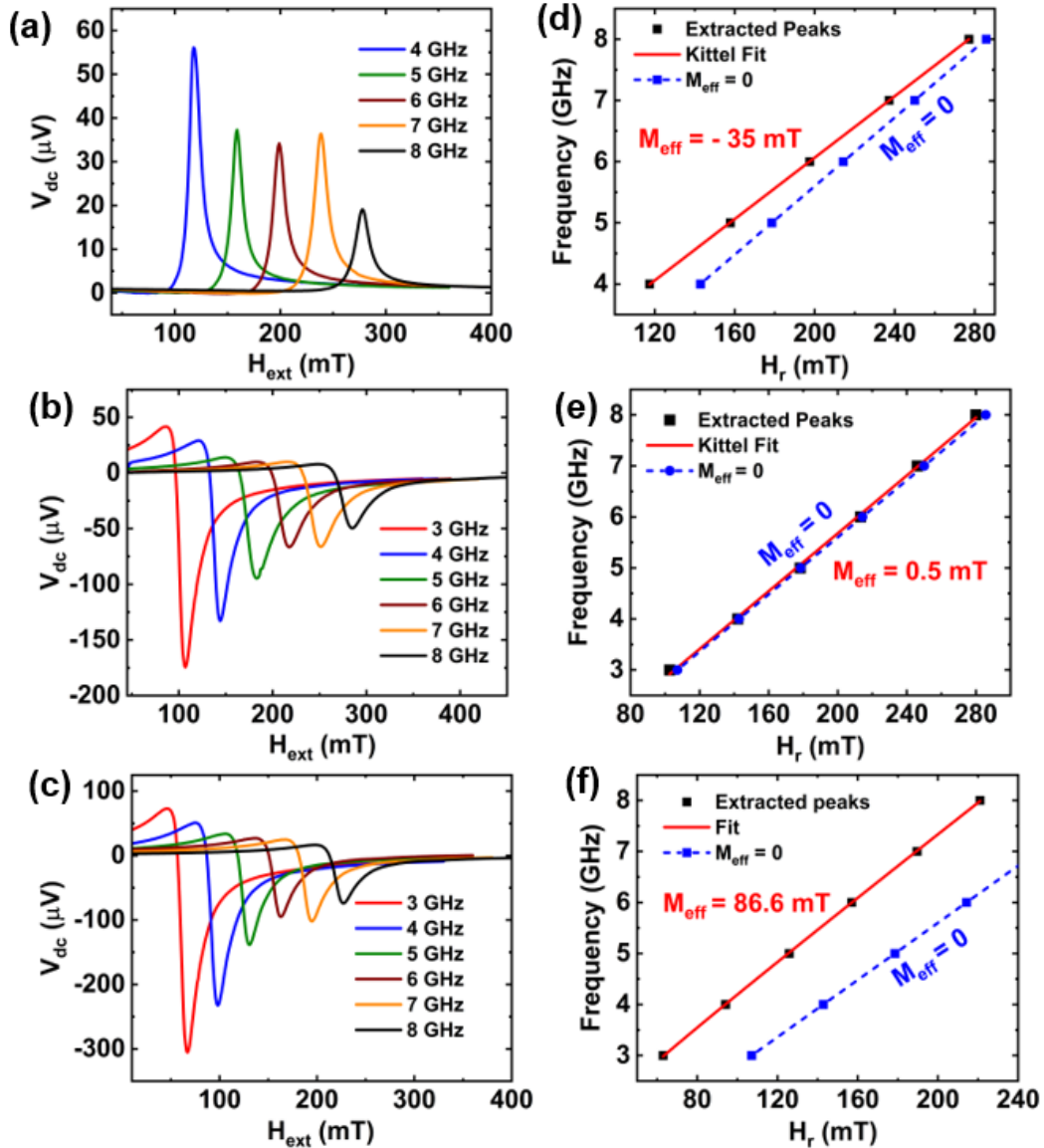

FIG. 3. Spin diode resonance plots at different injected microwave frequencies for (a) PMA, (b) compensated and (c) IPA stacks based microstrip waveguides. Resonance frequency as a function of the resonance field for (d) PMA, (e) compensated and (f) IPA stacks based microstrip waveguides. Solid red lines are Kittel fits and dotted blue lines, plotted for guidance, corresponds to $M_{eff} = 0$.
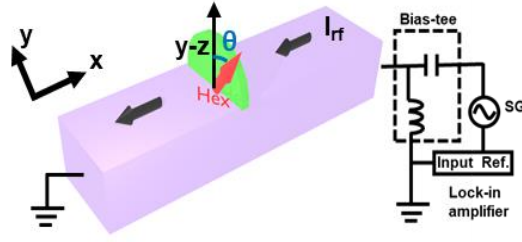
FIG. 4. Schematic illustration of spin-diode measurement set-up when external field is rotated out-of-plane.

devices. Clearly, the compensated stack-based device is closest to the near zero effective anisotropy.

Given that the first order anisotropy is close to zero in the compensated device, the possible influence of the second order anisotropy needs to be taken into consideration. The following equations are the more generalized forms which take the second order anisotropy into consideration,

$$f = \gamma/2\pi(H_1 H_2)^{1/2} \tag{3}$$

with

$$H_1 = H_r \cos(\theta_H - \theta_M) + H_{k1}^{eff} \cos^2\theta_M - H_{k2}\cos^4\theta_M,$$
$$H_2 = H_r \cos(\theta_H - \theta_M) + H_{k1}^{eff}\cos 2\theta_M - H_{k2}/2(\cos 2\theta_M + \cos 4\theta_M), \tag{4}$$

where θ_H, θ_M correspond to the angle of the external magnetic field and the magnetization angle measured from the sample normal, respectively. H_{k1}^{eff} and H_{k2} correspond to the first and the second order effective anisotropy fields, respectively [43]. By adopting H_{k1}^{eff}, H_{k2} and γ as adjustable parameters, the θ_H dependence of H_r yields the first and the second order anisotropy fields. The energy minimum conditions $\partial F/\partial\theta_M = 0$ and $\partial^2 F/\partial\theta_M^2 > 0$ are used to extract the value for θ_M, where F is the magnetic energy density [43].

Spin-diode measurements are performed by sweeping the magnetic field at different out-of-plane angles, θ_H, in the y-z plane as shown in the schematic of Figure 4. In this geometry, the signal strength of the output voltage is larger due to the spin pumping contributions [44]. The resonance fields, H_r, are extracted from the sum of symmetric and antisymmetric Lorentzians for each of the angles. The measurements are first performed for the IPA and the

8

PMA devices. The extracted H_r as a function of θ_H are shown in Figures 5 (a) and (b), with input microwave frequencies fixed at 3 GHz and 4 GHz for the IPA and the PMA devices, respectively. The curves display a monotonic behaviour, where the H_r is minimum close to the in-plane angle ($\theta_H = \pm 90$ deg) for the IPA device and close to the out-of-plane angle ($\theta_H = 0$ deg) for the PMA device. The nature of the curves is independent of the input microwave frequency, different values are selected for the two devices based on the signal quality. The measurements have been performed for the compensated device at a frequency of 5 GHz and the corresponding H_r vs θ_H plots are shown in Figure 5 (c). The curves display a non-monotonic behaviour, where the H_r is minimum at an intermediate angle close to 50 deg. This is referred to as the cone angle and its existence is an indication of compensation of the anisotropy [34,45]. The curves are well fit with (4) and are used to extract $H_{k1}^{eff} = -0.8$ mT and $H_{k2} = 0.47$ mT. The obtained parameters also satisfy the following conditions for the existence of an easy cone: $H_{k1}^{eff} < 0$; $H_{k2} > 0$ and $H_{k2} > -H_{k1}^{eff}/2$ [34]. These measurements, thus demonstrate that a device with compensated anisotropy has been fabricated. It would be further employed to demonstrate fixed frequency applications.
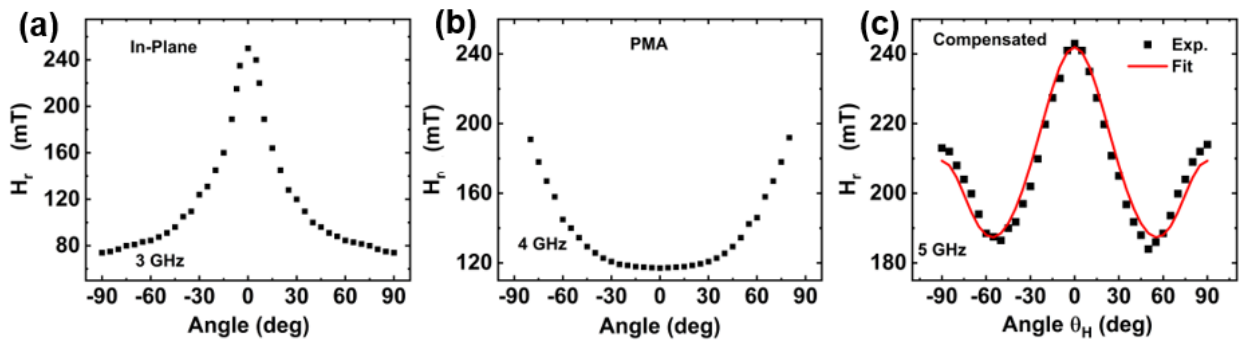

FIG. 5. Resonance field vs field angle for the microstrip waveguide with (a) IPA stack, microwave frequency fixed at 3 GHz (b) PMA stack, microwave frequency fixed at 4 GHz and (c) compensated stack, microwave frequency fixed at 5 GHz.

C. Input independent spin-Hall diode with fixed frequency

A synapse can be realized using spin-diodes. Leroux *et al*. demonstrated a MAC operation using magnetic tunnel junctions as spin diodes [22]. In a MAC operation, the output voltage U_j can be represented by a weighted sum of the input power, $U_j = \Sigma P_i W_{ji}$. The above equation can be mapped to a spin-diode equation in the linear zone close to resonance, where the weights are represented by the resonator frequencies. During the frequency multiplexing in a MAC operation, each injected input power P_i, should be able to uniquely address the corresponding synapse by its frequency. This imposes a constraint on the frequency of the synapse which should not change with the injected rf power. In a spintronic resonator, this criterion is usually not satisfied on account of the inherent non-linearity. However, the compensated spin diode has the potential to function as an input independent synapse with a fixed frequency. Figure 6 (a)
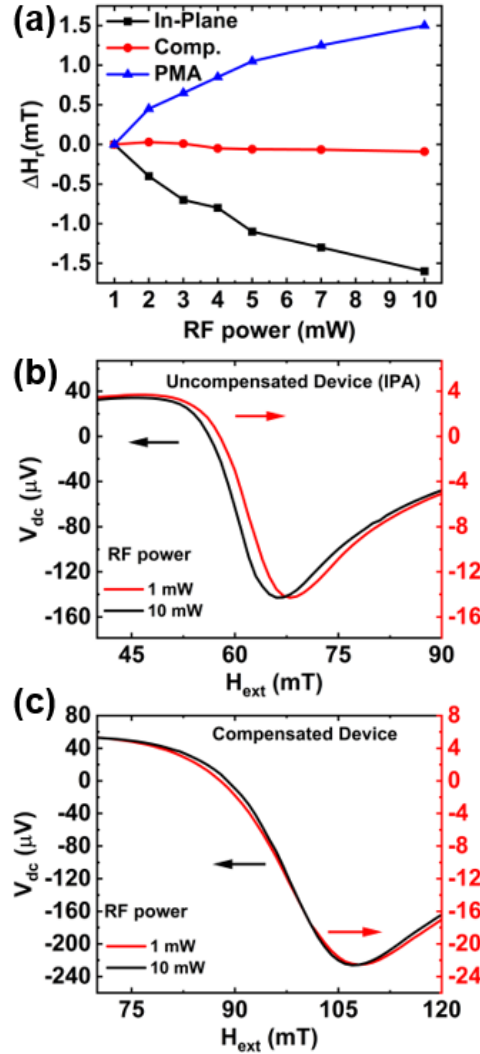

FIG. 6. (a) Comparison of shift in resonance field as a function of input rf power for a spin diode in IPA, compensated and PMA configuration. (b) Resonance curves as a function of input rf power for (b) IPA and (c) compensated (synapse) spin diodes

shows the shift in H_r as a function of the injected input rf power for the IPA, the compensated and the PMA spin diodes. Starting at the minimum input power (= 1 mW), the shift is normalized to 0 for all the three devices. As the input power is increased, the IPA and the PMA devices exhibit an increase in the shift of H_r, whereas, the compensated device shows a negligible shift in H_r. Figure 6 (b) and (c) show the comparison of the resonance plots for the IPA and the compensated devices, respectively, as a function of the input power. Clearly, there is no visible shift in the resonance field and the equivalent frequency with the injected rf power for the compensated device as compared to the IPA device. Thus, the compensated spin diode has the potential to function as an input independent spin-Hall synapse.

III. AUTO-OSCILLATIONS IN COMPENSATED SPIN HALL DEVICES – FIXED FREQUENCY AND LOW LINEWIDTH

A. Device fabrication and measurement set-up

Nano-constrictions with widths of 100 nm and 200 nm are fabricated on the compensated Co/Ni stacks using electron-beam lithography and Ar ion beam etching. Ti (15 nm)/Au (150 nm) metal stacks are deposited as electrodes and patterned into coplanar waveguides overlaying the nano-constrictions using optical lithography and lift-off. The device geometry is similar to the one used in previous reports for realizing an SHNO [30,31]. As a comparison, in-plane SHNO based on Py/Pt stacks are also patterned into nano-constrictions (Py = Permalloy = $Ni_{81}Fe_{19}$).

The scanning electron microscopy image of a 200 nm nano-constriction along with the measurement set-up to detect the auto-oscillations is shown in Figure 7 (a). A dc current, I_{dc}, is
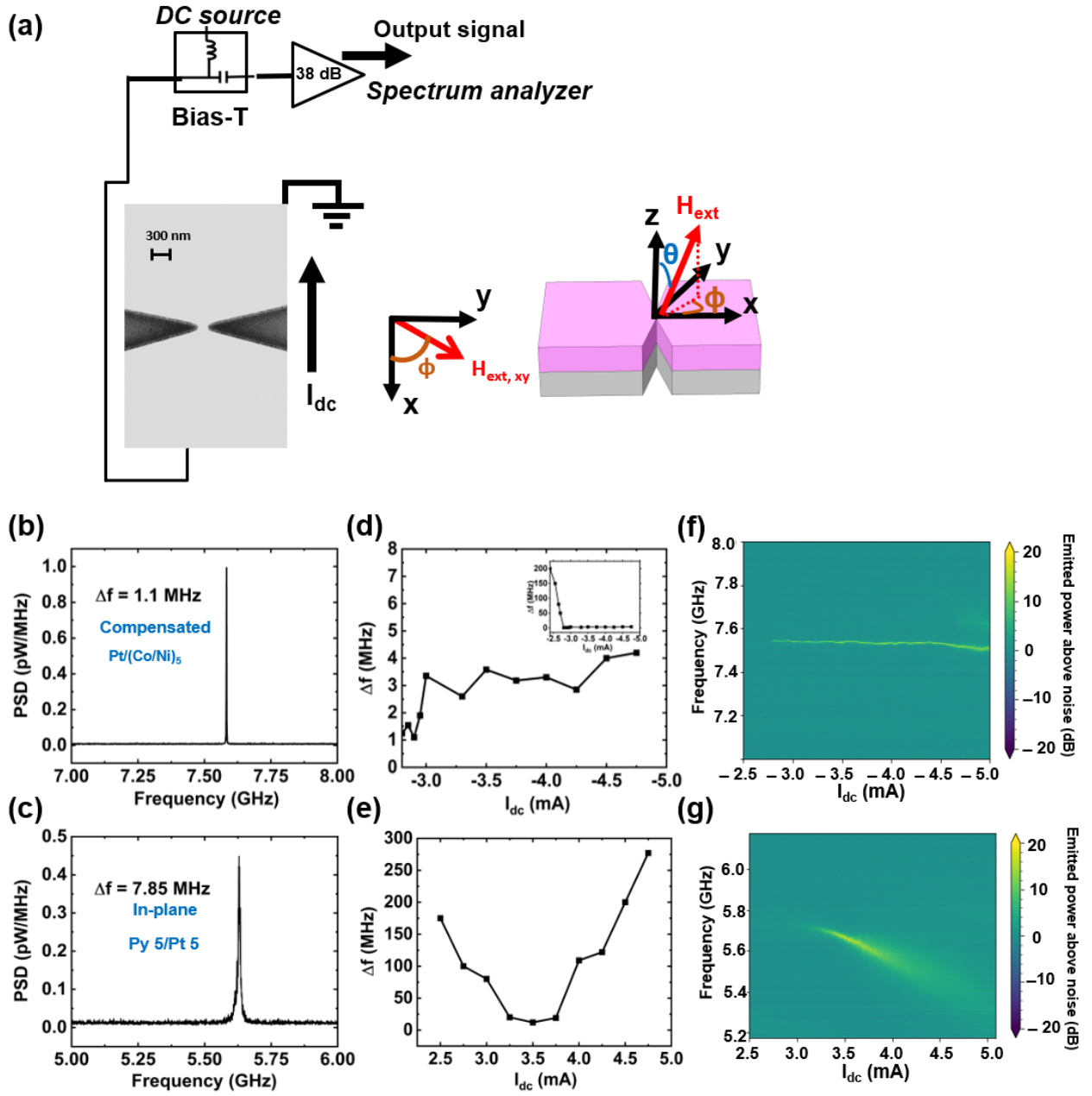
FIG. 7. (a) SEM image of 200 nm nano-constriction and a schematic to study the microwave emission from the SHNO. (b) Auto-oscillation spectra for the compensated Co/Ni SHNO obtained at $I_{dc} = +2.8$ mA, $H_{ext} = 300$ mT ($\theta_H = 15$ deg, $\phi_H = 50$ deg). (c) Auto-oscillation spectra for the in-plane Py/Pt SHNO obtained at $I_{dc} = -3.5$ mA, $H_{ext} = 50$ mT ($\theta_H = 85$ deg, $\phi_H = 42$ deg). Linewidth as a function of I_{dc} sweep for (d) compensated Co/Ni SHNO and (e) in-plane Py/Pt SHNO. Power spectral density plots showing frequency vs I_{dc} sweep for (f) compensated Co/Ni SHNO and (g) in-plane Py/Pt SHNO.

injected into the nano-constriction via the dc port of a bias-tee. An external magnetic field is applied at an in-plane angle, ϕ_H and an out-of-plane angle, θ_H. The SHNO emits microwave power which is extracted from the rf port of the bias-tee and amplified by 38 dB using a low noise wide-band amplifier. The output spectra are sampled using a spectrum analyzer. All measurements are performed at room temperature.

B. Electrical microwave measurements for compensated and in-plane devices

Figure 7 (b) shows the emission spectra for the 200 nm SHNO realized using the compensated Co/Ni stack at $I_{dc} = -2.8$ mA (+ x-direction) and $H_{ext} = 300$ mT ($\theta_H = 15$ deg, $\phi_H = 50$ deg). The linewidth (Δf) obtained from the Lorentz fit is 1.1 MHz with the peak power spectral density (PSD), after subtracting the amplifier gain, as high as 1 pW/MHz. To the best of our knowledge, the quality factor (Q ≈ 7500) obtained is more than the highest reported using a single constriction based SHNO [18,46]. As a comparison, the above measurements are also performed on Py/Pt based SHNO devices. Figure 7 (c) shows the corresponding spectra obtained at $I_{dc} = +3.5$ mA and $H_{ext} = 50$ mT ($\theta_H = 85$ deg, $\phi_H = 42$ deg). The field orientation is maintained close to the in-plane direction for this device to excite the in-plane modes. In this case, the sign of I_{dc} is positive as the SOT is from the top interface, whereas for the Pt/Co/Ni multilayers the sign of I_{dc} is negative, since the SOT is from the bottom interface. The minimum linewidth obtained from the Lorentz fit is 7.85 MHz and is much larger than that achieved using the compensated Co/Ni SHNO. The above observations can be explained from (2), which indicate a reduction of Δf if N is reduced. To further validate this claim, we sweep the injected I_{dc} and record the variation of the frequency and Δf for the two SHNOs at the above-mentioned external fields and orientations, respectively. Figures 7 (d) and (e) show Δf as a function of I_{dc} for the compensated Co/Ni and the in-plane Py/Pt SHNOs, respectively. Figure 7 (d) is plotted for I_{dc} larger than the critical current of auto-oscillations ($I_c = -2.7$ mA), which is the region of interest, and the inset shows the data for $I < I_c$ as well. When $I_{dc} < I_c$, Δf increases with the reduction in current for both the devices, as expected. At large I_{dc}, the Py/Pt SHNO shows an increase in Δf due to the inherent non-linearity, which is not the case with the compensated Co/Ni SHNO which shows a near constant Δf. The evidence for the absence of non-linearity in the compensated Co/Ni SHNO becomes stronger when we compare its frequency vs I_{dc} shown in the power spectral density plots in Figure 7 (f) to that obtained for Py/Pt SHNO in Figure 7 (g). Clearly, the rate of change of frequency with the current (df/dI) is minimal for the compensated Co/Ni SHNO (= 10 MHz/ mA) and significant for the in-plane
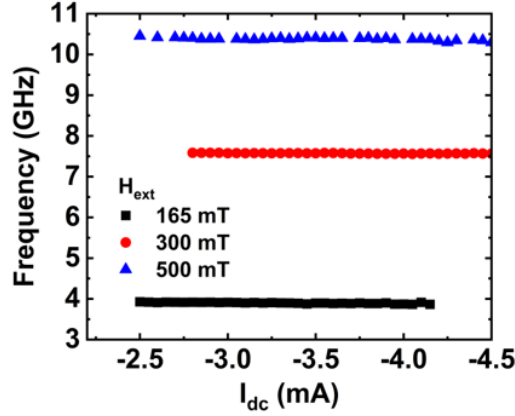
FIG. 8. Auto-oscillation frequency as a function of I_{dc} sweep for compensated Co/Ni SHNO performed at external fields of 165 mT, 300 mT and 500 mT.

Py/Pt SHNO (= 500 MHz/mA). However, for $I_{dc} > -4.5$ mA, some non-linearity can be observed in Figure 7 (f), which could be ascribed to the device heating or frequency shift due to the Oersted field or the field-like torque [39]. The above observations are a direct validation of a reduction in the non-linearity as indicated in (1). The measurements are repeated at different
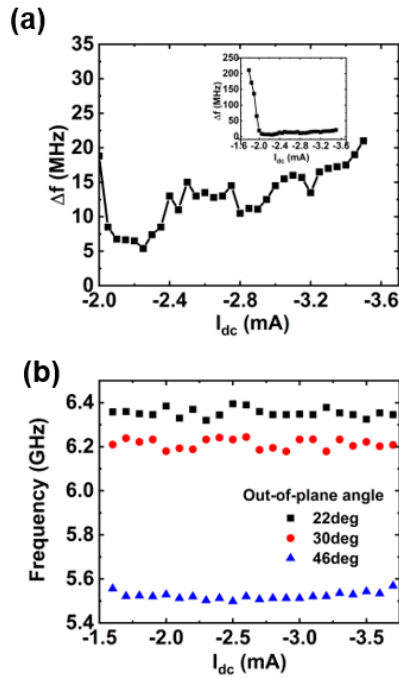

FIG. 9. (a) Linewidth as a function of I_{dc} sweep at $H_{ext} = 180$ mT ($\theta_H = 15$ deg, $\phi_H = 50$ deg) for the compensated Co/Ni SHNO with 100 nm width. (b) Comparison of frequency vs I_{dc} sweep when $H_{ext} = 180$ mT is applied along out-of-plane angles of 22, 30 and 46 deg to the 100 nm compensated Co/Ni SHNO

applied external magnetic fields to the compensated Co/Ni SHNO and are shown in Figure 8. As is the case, the external fields only change the frequency of the ferromagnetic resonance and not the slope which are nearly zero for the compensated Co/Ni SHNO.

To further validate the existence of compensation across different devices, the measurements are repeated on a 100 nm constriction. Figure 9 (a) shows the variation of Δf vs I_{dc} for this device, performed at H_{ext} = 180 mT (θ_H = 15 deg, ϕ_H = 50 deg). The plot indicates a high Δf for $I_{dc} < I_c$ (= − 1.8 mA), as shown in the inset, upon which it does not increase significantly at higher currents. A larger Δf in excess of 5 MHz as opposed to 1.1 MHz is obtained when the width of the constriction is reduced from 200 to 100 nm, which is expected due to a smaller mode volume. We also performed frequency vs I_{dc} for this device at different orientations of the external magnetic field (H_{ext} = 180 mT). The measurements are performed for three different angles, θ_H = 22, 30 and 46 degrees, respectively keeping ϕ_H fixed at 90 deg. Figure 9 (b) shows the results of frequency vs I_{dc} at different out-of-plane angles of the external field. At each angle, the frequency is different as expected, and is minimum at 46 deg which is close to the cone angle of precession. However, the frequency remains nearly constant with respect to I_{dc}, even at different angles, thus providing a strong evidence for the absence of non-linearity in the compensated SHNO device.

The results above highlight notable differences in device properties and oscillation conditions for the 200 nm and 100 nm width nano-constrictions. These variations in width lead to distinct internal fields due to geometry and fabrication-related variability. Factors such as shape-induced anisotropy modification and etch-induced reduction of PMA affect smaller nano-constrictions more significantly [47]. Consequently, different fields and applied angles alter the effective fields, resulting in dissimilar oscillation frequencies for the two widths. Furthermore, the effective anisotropy for nano-constriction geometries of varying widths would also differ.

In a previous estimation, the M_{eff} for the micron-sized device was calculated to be 0.5 mT (Figure 3(e)). To estimate the M_{eff} in nano-constrictions, we conducted spin-diode measurements on the 100 nm and 200 nm nano-constrictions using the methods outlined in [48]. The M_{eff} values were determined to be +9.4 mT and +5.2 mT for 100 nm and 200 nm nano-constrictions, respectively. As anticipated, these values are significantly larger than the estimated value for the microstrip (0.5 mT). The positive sign suggests a reduction of PMA, with the 100 nm nano-constriction exhibiting weaker PMA. Nevertheless, the effective anisotropy remains an order of magnitude lower than previously reported values [48] and continues to display reduced frequency tunability with current.

It should be noted that the data presented for minimum linewidths represent the best device obtained. However, factors such as device-to-device variability, as previously discussed, and fabrication process artifacts can also influence the minimum linewidths across different devices with the same widths. Furthermore, Joule heating and current-induced Oersted fields could impact the results. We conducted measurements for five different devices for each nominal width of the nano-constriction, with details provided in Supplemental Material [49]. The linewidth for the 100 nm nano-constriction is determined to be 6.2 ± 1.8 MHz, while for the 200 nm nano-constriction it is found to be 1.8 ± 0.6 MHz. Although the effects of device-to-device variability are more pronounced near anisotropy compensation, the obtained linewidths are considerably lower than those reported for uncompensated Co/Ni-based PMA oscillator devices [50,51].

IV. CONCLUSION

In this work, we experimentally demonstrate a significant reduction of non-linearity in the magnetization dynamics of an SHNO by compensating its effective magnetic anisotropy using Co/Ni multilayers with a Pt heavy metal. By tuning the thicknesses of Co and Ni, we were able to obtain an easy cone anisotropy for the compensated stack when the perpendicular magnetic anisotropy was counterbalanced by the demagnetization field. The spin-diode signal is shown to be independent of the input power, making it a promising candidate for synapses in neuromorphic computing applications.

We also investigated auto-oscillations in the compensated SHNO using nano-constrictions and compared them with Py/Pt based SHNOs with an in-plane anisotropy. Our results demonstrate that the frequency and linewidth of the compensated SHNO are independent of the applied dc current, external fields, and orientations, with a linewidth as low as 1.1 MHz and a peak emission power as high as 1 pW/MHz. This indicates the possibility of realizing nano-oscillators with improved device performance, potentially reducing phase noise by decoupling amplitude noise from it.

Our study also opens up possibilities for neuromorphic applications such as frequency multiplexing in a multiply-and-accumulate operation. The compensated SHNO could function as a neuron of low linewidth and a fixed frequency, uniquely addressing a compensated spin diode as a synapse. Additionally, it opens up prospects for generating voltage spikes emulating spike-based neurons by exploiting easy-plane oscillations in a compensated SHNO. These

findings suggest exciting prospects for the development of neuromorphic devices with improved performance and functionality.

ACKNOWLEDGMENTS

[1]   J. C. Slonczewski, *Current-Driven Excitation of Magnetic Multilayers*, J Magn Magn Mater **159**, L1 (1996).

[2]   L. Berger, *Emission of Spin Waves by a Magnetic Multilayer Traversed by a Current*, Phys Rev B **54**, 9353 (1996).

[3]   S. I. Kiselev, J. C. Sankey, I. N. Krivorotov, N. C. Emley, R. J. Schoelkopf, R. A. Buhrman, and D. C. Ralph, *Microwave Oscillations of a Nanomagnet Driven by a Spin-Polarized Current*, Nature **425**, 380 (2003).

[4]   V. E. Demidov, S. Urazhdin, H. Ulrichs, V. Tiberkevich, A. Slavin, D. Baither, G. Schmitz, and S. O. Demokritov, *Magnetic Nano-Oscillator Driven by Pure Spin Current*, Nat Mater **11**, 1028 (2012).

[5]   A. Slavin and V. Tiberkevich, *Nonlinear Auto-Oscillator Theory of Microwave Generation by Spin-Polarized Current*, IEEE Trans Magn **45**, 1875 (2009).

[6]   A. N. Slavini and P. Kabos, *Approximate Theory of Microwave Generation in a Current-Driven Magnetic Nanocontact Magnetized in an Arbitrary Direction*, IEEE Trans Magn **41**, 1264 (2005).

[7]   M. Dvornik, A. A. Awad, and J. Åkerman, *Origin of Magnetization Auto-Oscillations in Constriction-Based Spin Hall Nano-Oscillators*, Phys Rev Appl **9**, (2018).

[8]   M. Zahedinejad, A. A. Awad, P. Dürrenfeld, A. Houshang, Y. Yin, P. K. Muduli, and J. Åkerman, *Current Modulation of Nanoconstriction Spin-Hall Nano-Oscillators*, IEEE Magn Lett **8**, 1 (2017).

[9]   P. K. Muduli, Ye. Pogoryelov, S. Bonetti, G. Consolo, F. Mancoff, and J. Åkerman, *Nonlinear Frequency and Amplitude Modulation of a Nanocontact-Based Spin-Torque Oscillator*, Phys Rev B **81**, 140408 (2010).

[10]   M. R. Pufall, W. H. Rippard, S. Kaka, T. J. Silva, and S. E. Russek, *Frequency Modulation of Spin-Transfer Oscillators*, Appl Phys Lett **86**, 082506 (2005).

[11]   A. Litvinenko, A. Sidi El Valli, V. Iurchuk, S. Louis, V. Tyberkevych, B. Dieny, A. N. Slavin, and U. Ebels, *Ultrafast GHz-Range Swept-Tuned Spectrum Analyzer with 20 Ns Temporal Resolution Based on a Spin-Torque Nano-Oscillator with a Uniformly Magnetized "Free" Layer*, Nano Lett **22**, 1874 (2022).

[12] A. Litvinenko, P. Sethi, C. Murapaka, A. Jenkins, V. Cros, P. Bortolotti, R. Ferreira, B. Dieny, and U. Ebels, *Analog and Digital Phase Modulation and Signal Transmission with Spin-Torque Nano-Oscillators*, Phys Rev Appl **16**, (2021).

[13] A. Litvinenko et al., *Ultrafast Sweep-Tuned Spectrum Analyzer with Temporal Resolution Based on a Spin-Torque Nano-Oscillator*, Nano Lett **20**, 6104 (2020).

[14] R. Sharma, R. Mishra, T. Ngo, Y. X. Guo, S. Fukami, H. Sato, H. Ohno, and H. Yang, *Electrically Connected Spin-Torque Oscillators Array for 2.4 GHz WiFi Band Transmission and Energy Harvesting*, Nat Commun **12**, (2021).

[15] H. S. Lee, S. H. Kim, T. H. Jang, H. G. Park, B. C. Min, S. Y. Park, and C. S. Park, *Power-Efficient Spin-Torque Nano-Oscillator-Based Wireless Communication with CMOS High-Gain Low-Noise Transmitter and Receiver*, IEEE Trans Magn **55**, (2019).

[16] S. Tsunegi, T. Taniguchi, K. Nakajima, S. Miwa, K. Yakushiji, A. Fukushima, S. Yuasa, and H. Kubota, *Physical Reservoir Computing Based on Spin Torque Oscillator with Forced Synchronization*, Appl Phys Lett **114**, (2019).

[17] M. Romera et al., *Binding Events through the Mutual Synchronization of Spintronic Nano-Neurons*, Nat Commun **13**, (2022).

[18] M. Zahedinejad, A. A. Awad, S. Muralidhar, R. Khymyn, H. Fulara, H. Mazraati, M. Dvornik, and J. Åkerman, *Two-Dimensional Mutually Synchronized Spin Hall Nano-Oscillator Arrays for Neuromorphic Computing*, Nat Nanotechnol **15**, 47 (2020).

[19] M. Romera et al., *Vowel Recognition with Four Coupled Spin-Torque Nano-Oscillators*, Nature **563**, 230 (2018).

[20] D. C. Ralph and M. D. Stiles, *Spin Transfer Torques*, J Magn Magn Mater **320**, 1190 (2008).

[21] A. Ross et al., *Multilayer Spintronic Neural Networks with Radio-Frequency Connections*, ArXiv Preprint ArXiv:2211.03659 (2022).

[22] N. Leroux, D. Marković, E. Martin, T. Petrisor, D. Querlioz, A. Mizrahi, and J. Grollier, *Radio-Frequency Multiply-and-Accumulate Operations with Spintronic Synapses*, Phys Rev Appl **15**, (2021).

[23] M. W. Keller, M. R. Pufall, W. H. Rippard, and T. J. Silva, *Nonwhite Frequency Noise in Spin Torque Oscillators and Its Effect on Spectral Linewidth*, Phys Rev B **82**, 54416 (2010).

[24] D. Marković, M. W. Daniels, P. Sethi, A. D. Kent, M. D. Stiles, and J. Grollier, *Easy-Plane Spin Hall Nano-Oscillators as Spiking Neurons for Neuromorphic Computing*, Phys Rev B **105**, (2022).

[25] S. Jiang, R. Khymyn, S. Chung, T. Q. Le, L. H. Diez, A. Houshang, M. Zahedinejad, D. Ravelosona, and J. Åkerman, *Reduced Spin Torque Nano-Oscillator Linewidth Using He + Irradiation*, Appl Phys Lett **116**, (2020).

[26] E. Saitoh, M. Ueda, H. Miyajima, and G. Tatara, *Conversion of Spin Current into Charge Current at Room Temperature: Inverse Spin-Hall Effect*, Appl Phys Lett **88**, (2006).

[27] L. Liu, T. Moriyama, D. C. Ralph, and R. A. Buhrman, *Spin-Torque Ferromagnetic Resonance Induced by the Spin Hall Effect*, Phys Rev Lett **106**, 36601 (2011).

[28] J. E. Hirsch, *Spin Hall Effect*, Phys Rev Lett **83**, 1834 (1999).

[29] H. Mazraati, S. Chung, A. Houshang, M. Dvornik, L. Piazza, F. Qejvanaj, S. Jiang, T. Q. Le, J. Weissenrieder, and J. Åkerman, *Low Operational Current Spin Hall Nano-Oscillators Based on NiFe/W Bilayers*, Appl Phys Lett **109**, 242402 (2016).

[30] V. E. Demidov, S. Urazhdin, A. Zholud, A. v. Sadovnikov, and S. O. Demokritov, *Nanoconstriction-Based Spin-Hall Nano-Oscillator*, Appl Phys Lett **105**, (2014).

[31] B. Divinskiy, V. E. Demidov, A. Kozhanov, A. B. Rinkevich, S. O. Demokritov, and S. Urazhdin, *Nanoconstriction Spin-Hall Oscillator with Perpendicular Magnetic Anisotropy*, Appl Phys Lett **111**, (2017).

[32] B. Divinskiy, S. Urazhdin, S. O. Demokritov, and V. E. Demidov, *Controlled Nonlinear Magnetic Damping in Spin-Hall Nano-Devices*, Nat Commun **10**, (2019).

[33] A. A. Timopheev, R. Sousa, M. Chshiev, H. T. Nguyen, and B. Dieny, *Second Order Anisotropy Contribution in Perpendicular Magnetic Tunnel Junctions*, Sci Rep **6**, (2016).

[34] A. Okada, S. Kanai, S. Fukami, H. Sato, and H. Ohno, *Electric-Field Effect on the Easy Cone Angle of the Easy-Cone State in CoFeB/MgO Investigated by Ferromagnetic Resonance*, Appl Phys Lett **112**, (2018).

[35] B. M. S. Teixeira, A. A. Timopheev, N. Caçoilo, S. Auffret, R. C. Sousa, B. Dieny, and N. A. Sobolev, *Stabilization of the Easy-Cone Magnetic State in Free Layers of Magnetic Tunnel Junctions*, Phys Rev B **100**, (2019).

[36] G. H. O. Daalderop, P. J. Kelly, and F. J. A. den Broeder, *Prediction and Confirmation of Perpendicular Magnetic Anisotropy in Co/Ni Multilayers*, Phys Rev Lett **68**, 682 (1992).

[37] P. Sethi, C. Murapaka, G. J. Lim, and W. S. Lew, *In-Plane Current Induced Domain Wall Nucleation and Its Stochasticity in Perpendicular Magnetic Anisotropy Hall Cross Structures*, Appl Phys Lett **107**, 192401 (2015).

[38] S. Fukami, Y. Nakatani, T. Suzuki, K. Nagahara, N. Ohshima, and N. Ishiwata, *Relation between Critical Current of Domain Wall Motion and Wire Dimension in Perpendicularly Magnetized Co/Ni Nanowires*, Appl Phys Lett **95**, 232504 (2009).

[39] N. Figueiredo-Prestes et al., *Magnetization Switching and Deterministic Nucleation in Co/Ni Multilayered Disks Induced by Spin–Orbit Torques*, Appl Phys Lett **119**, 032410 (2021).

[40] A. A. Tulapurkar, Y. Suzuki, A. Fukushima, H. Kubota, H. Maehara, K. Tsunekawa, D. D. Djayaprawira, N. Watanabe, and S. Yuasa, *Spin-Torque Diode Effect in Magnetic Tunnel Junctions*, Nature **438**, 339 (2005).

[41] J. G. Choi, J. Park, M. G. Kang, D. Kim, J. S. Rieh, K. J. Lee, K. J. Kim, and B. G. Park, *Voltage-Driven Gigahertz Frequency Tuning of Spin Hall Nano-Oscillators*, Nat Commun **13**, (2022).

[42] J.-M. Beaujour, D. Ravelosona, I. Tudosa, E. E. Fullerton, and A. D. Kent, *Ferromagnetic Resonance Linewidth in Ultrathin Films with Perpendicular Magnetic Anisotropy*, Phys Rev B **80**, 180415 (2009).

[43] A. Okada, S. Kanai, M. Yamanouchi, S. Ikeda, F. Matsukura, and H. Ohno, *Electric-Field Effects on Magnetic Anisotropy and Damping Constant in Ta/CoFeB/MgO Investigated by Ferromagnetic Resonance*, Appl Phys Lett **105**, (2014).

[44] A. Okada, Y. Takeuchi, K. Furuya, C. Zhang, H. Sato, S. Fukami, and H. Ohno, *Spin-Pumping-Free Determination of Spin-Orbit Torque Efficiency from Spin-Torque Ferromagnetic Resonance*, Phys Rev Appl **12**, (2019).

[45] Y. Fu, I. Barsukov, J. Li, A. M. Gonçalves, C. C. Kuo, M. Farle, and I. N. Krivorotov, *Temperature Dependence of Perpendicular Magnetic Anisotropy in CoFeB Thin Films*, Appl Phys Lett **108**, (2016).

[46] T. Chen, R. K. Dumas, A. Eklund, P. K. Muduli, A. Houshang, A. A. Awad, P. Dürrenfeld, B. G. Malm, A. Rusu, and J. Åkerman, *Spin-Torque and Spin-Hall Nano-Oscillators*, Proceedings of the IEEE **104**, 1919 (2016).

[47] H. Fulara, M. Zahedinejad, R. Khymyn, A. A. Awad, S. Muralidhar, M. Dvornik, and J. Åkerman, *Spin-Orbit Torque-Driven Propagating Spin Waves*, Sci Adv **5**, (2019).

[48] H. Fulara, M. Zahedinejad, R. Khymyn, M. Dvornik, S. Fukami, S. Kanai, H. Ohno, and J. Åkerman, *Giant Voltage-Controlled Modulation of Spin Hall Nano-Oscillator Damping*, Nat Commun **11**, (2020).

[49] *See Supplemental Material at [] for Linewidth Variation across Different Devices for the Same Width Nano-Constrictions*.

[50] B. Divinskiy, V. E. Demidov, A. Kozhanov, A. B. Rinkevich, S. O. Demokritov, and S. Urazhdin, *Nanoconstriction Spin-Hall Oscillator with Perpendicular Magnetic Anisotropy*, Appl Phys Lett **111**, 032405 (2017).

[51] R. H. Liu, W. L. Lim, and S. Urazhdin, *Dynamical Skyrmion State in a Spin Current Nano-Oscillator with Perpendicular Magnetic Anisotropy*, Phys Rev Lett **114**, 137201 (2015).